Preprint LA-UR-00-4101

Title: STRUCTURAL ANALYSIS OF ARGONNE NATIONAL LABORATORY 3-GAP, 350 MHz, Bg=.36 SPOKE RESONATOR CAVITY

Author(s): Richard P. LaFave LANSCE-1

Submitted To: Informal Distribution - Internal and External

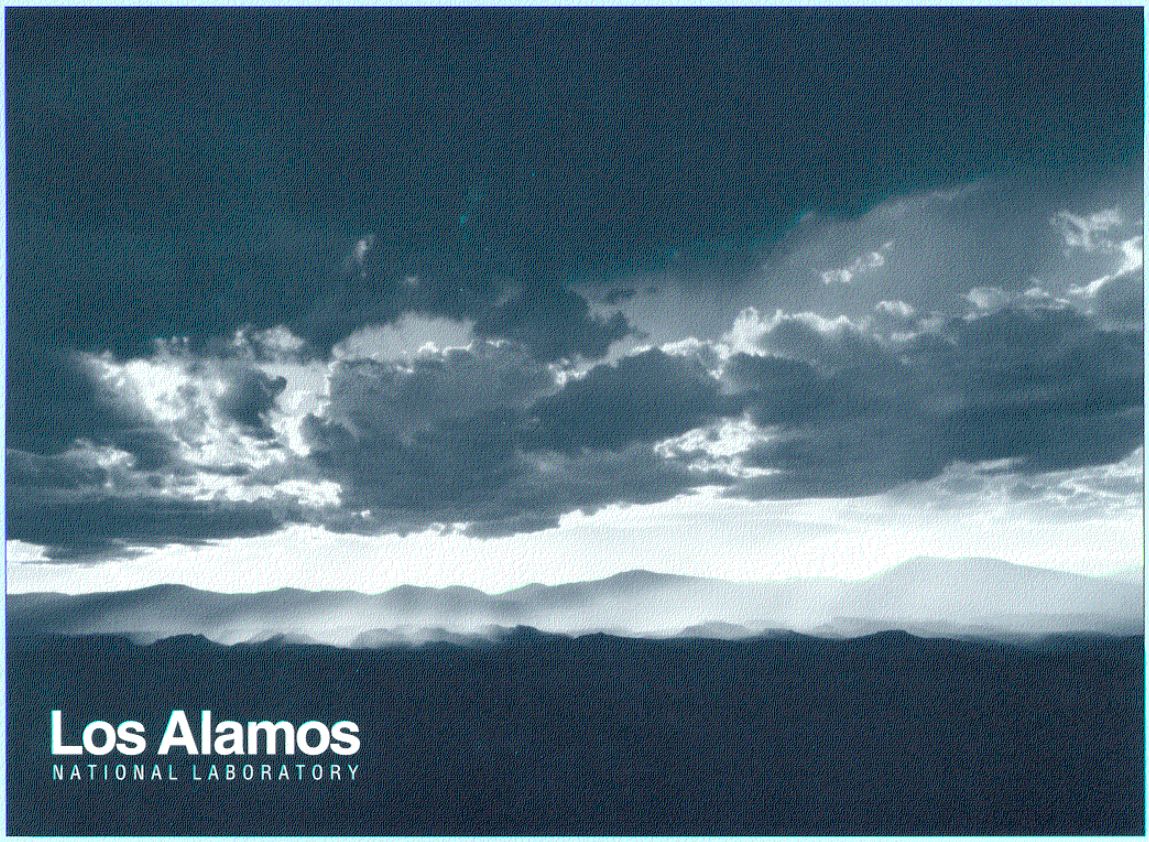

Photograph by Chris J. Lindberg

Los Alamos
NATIONAL LABORATORY

memorandum
LANSCE Division
Group LANSCE-1

To/MS: Dale Schrage, MS H817
From/MS: Richard LaFave, MS H817 RPL
Phone/FAX: 5-0029/5-2904
Symbol: LANSCE-1:00-69
Date: August 14, 2000
Email: rpl@lanl.gov

SUBJECT: Structural Analysis of Argonne National Laboratory 3-gap, 350 MHz, β_g = .36 Spoke Resonator Cavity

Introduction:

As we discussed, a finite element model of the Argonne National Laboratory 3-gap, 350 MHz, β_g=.36 spoke resonator cavity has been developed. This memo summarizes the model predictions for peak stresses, deflections, and flange reaction forces under vacuum loads at room temperature, and also for forces required to produce a specified tuning deflection. The results shown in Table 2 summarize the model predictions for the various load conditions and geometries considered. Material properties were taken as the ambient temperature niobium properties listed in Table 3 of LA-UR # 99-5826.

Models:

Models of the 3-gap, 350 MHz, β_g =.36 spoke resonator have been constructed for COSMOS/M and represent the cavity geometry as defined in Argonne drawing EB-24003-X, dated February 28, 2000, which is reproduced in Figure 19. In addition to the geometry as defined in the drawing, variations in geometry were also considered. They were:

a) The addition of an annular end wall stiffener.

b) Changing the geometry of the radial end wall stiffeners to wrap around the outer diameter of the main body.

c) Changing the radial end wall stiffener cross-section to a 'T'.

d) Changing the wall thickness from 3 mm to 4 mm.

Figure 1 shows the cavity geometry as defined by Argonne drawing EB-24003-X, while Figure 2 shows the geometry with all of the additions mentioned above.

Material properties were taken as the ambient temperature niobium properties listed in Table 3 of LA-UR # 99-5826 and are reproduced in Table 1.

Table 1: Room Temperature Properties of Niobium

Property	Value	Units
Density, ρ	0.31	lb/in^3
Modulus, E	$1.42X10^7$	lb/in^2
Yield Strength, σ_y	7000	lb/in^2
Poisson's Ratio, ν	0.38	none

The models were meshed with three and four node shell elements resulting in problems with between 35,000 and 42,000 degrees of freedom. Figure 3 shows the mesh generated for the cavity as defined in Argonne drawing EB-24003-X. Figure 4 shows the mesh generated when all of the additions mentioned above were included. Figure 5 shows the mesh for a cavity with no endwall stiffeners. This model was used for result verification by comparing its predictions against a separate 2-D axi-symmetric model. This test is documented in Table 2, cases 31 and 32, and shows good agreement.

Model Verification:

Independent model verification was performed using two independently generated models. The first was an axi-symmetric model representing the case where no radial or annular endwall stiffeners are present. The results from this model were compared against the full model with all stiffeners removed. Figure 5 shows the resulting mesh for the full model with no stiffeners. Figures 14 and 15 show stress and displacement for the full model under these conditions with vacuum loading, while Figure 16 shows the predictions from the axi-symmetric model with vacuum loading. Results for both models are tabulated in Table 2, cases 31 and 32, and show good agreement. The second independent model was of a symmetric pie slice of the endwall with a radial endwall stiffener. Figures 17 and 18 show the results from this model under vacuum loading, while Figures 8 and 9 show results from the full model under similar conditions. Results for both models are summarized in Table 2, cases 4 and 33, and show good agreement.

Load Cases:

Three load cases were considered for the models:

a) A single end flange fixed and a specified displacement of 0.0010 inches at the other end flange. This load case was used to predict the forces required to produce a fixed tuning deflection. In Table 2 this load case is referred to as the "displaced end" case.

b) Both end flanges fixed and ambient pressure on all external surfaces. This load case was used to predict stresses and deflections while the cavity is under vacuum at ambient temperature and constrained in length. In Table 2 this load case is referred to as the "vacuum loading" case.

c) A single end flange fixed and ambient pressure on all external surfaces. This load case was used to predict stresses and deflections while the cavity is being leak checked. In Table 2 this load case is referred to as the "leak check" case.

Results and Discussion:

Results for each of the cases considered are tabulated in table 2. In addition, the "comments" entry in the table will refer the reader to the specific figures, if any, that depict the results for that case. Some results, for example case 1, Figure 6, show peak stresses at a single node at the end of each radial stiffener. In an effort to determine if this single value was an artifact of the model or a valid prediction the mesh was refined in this area and re-run. Predictions with the refined mesh showed the high stress still at a single node at the end of the stiffener, with the stress magnitude even higher. Although this would tend to indicate an anomalous prediction at that node the results given in Table 2 include these predictions.

Because of the variety of conditions represented in Table 2 some general comments are in order:

a) The leak check cases: None of the cases modeled indicate satisfactory performance under the conditions defined above as the leak check case. In all of these cases peak stresses are predicted to be in excess of the yield stress of 7000 psi for ambient temperature niobium. Because of these results it will be necessary to fix both end flanges when performing leak checking. Performing leak checking with both end flanges fixed will produce loads and deflections as given under the "vacuum loading" cases.

b) The annular endwall stiffener: The addition of an annular endwall stiffener does not have a significant impact on the stress levels in the structure. The annular stiffener does however reduce the peak displacements in the structure under load. As can be seen by reviewing cases 4 and 13 the addition of the annular stiffener reduced peak displacements from approximately 0.006 inches to 0.003 inches between the radial endwall stiffeners.

c) Wrap around ends on radial stiffeners: The addition of the wrap around ends on the radial stiffeners reduced the peak stresses in the structure. By reviewing the results from cases 1 and 4 the peak stresses are reduced from 5820 psi (84% of yield strength) to 4450 psi (64% of yield strength) with the addition of this feature. This is a significant improvement for the design margin of the structure.

d) T-section radial endwall stiffener: Changing the cross-section of the radial endwall stiffeners to a T section reduced the peak displacements under load. Small reductions in displacement can be seen by comparing cases 1 and 7 as well as cases 4 and 10.

e) Changing the wall thickness from 3 mm to 4 mm: Changing wall thickness from 3 mm to 4 mm significantly reduced both peak stress and displacements for all load cases considered. Reviewing cases 19 and 1 shows a reduction in stress from 5820 psi to 3420 psi with a reduction in peak displacements from .0059 inches to .0031 inches resulting from an increased wall thickness of 4 mm. Fabrication problems however make this an unattractive alternative.

Recommendations:

a) Leak checking of these structures should be performed with both end flanges fixed. Leak testing in this configuration generates the same loads, stresses, and deflections as defined in the vacuum loading case, which indicates satisfactory behavior.

b) Since the addition of the annular stiffener complicates the manufacture of the cavity, this option is not recommended unless or until it is determined that peak deflections of .006 inches between radial endwall stiffeners are not acceptable.

c) The addition of the wrap around ends on the radial stiffeners should be included in the design. The cost of the extra material and the penalty in manufacturing complexity are probably small compared to the structural benefits.

d) Changing the cross-section of the radial endwall stiffeners to a T section is not recommended unless or until it is determined that peak deflections of .006 inches between radial endwall stiffeners are not acceptable.

e) Changing the wall thickness to 4 mm is not recommended. Although the stress and displacement levels show significant improvement at the 4 mm wall thickness, the additional material expense and fabrication difficulties are major. Stress and displacement levels can be improved with less drastic measures.

Summary:

A structural analysis of the Argonne National Laboratory 3-gap, 350 MHz, β_g=.36 spoke resonator cavity has been performed in order to estimate the forces required to produce a specified tuning deflection and also to estimate stresses and deflections while under vacuum loads at room temperature. The results of these cases are presented in Table 2 and include cases to consider variations in wall thickness and the presence or absence of endwall stiffeners. The analysis indicates that the endwall stiffeners are necessary to limit stresses to below the yield point under vacuum loading conditions at room temperature. The analysis also indicates that the factor of safety for structural stress levels, $\sigma_{yield}/\sigma_{max}$, can be improved by about 40% by changing the design of the radial endwall stiffeners to wrap around the outer diameter of the main body.

Los Alamos National Laboratory
LANSCE Division
Group LANSCE-1
Table 2; Results from Analysis of ANL 350 MHz, 3-Gap, β_g=.36 Spoke Resonator

Case Number	Boundary Conditions / Loads			Radial Endwall Stiffeners				Annular Endwall Stiffener		Wall Thick	σ_{max} Von Mises	δ_{max}	Flange Reaction Force	Comments
	Vacuum Loading	Displaced End	Leak Check	ANL EB-24003-X	Wrap Around Tips	T-Section	None	Yes	No	(mm)	(psi)	(inches)	(lbs.)	
1	X			X					X	3	5,820	0.0059	1556	Figures 6 & 7 ; Stress & Displacement
2		X		X					X	3	361	0.0010	43	
3			X	X					X	3	11,318	0.0389	0	
4	X				X				X	3	4,450	0.0055	1518	Figures 8 & 9 ; Verification Problem - Compare to Case 33
5		X			X				X	3	372	0.0010	44	
6			X		X				X	3	10,818	0.0371	0	
7	X					X			X	3	6,845	0.0055	1463	Figures 10 & 11 ; Stress & Displacement
8		X				X			X	3	444	0.0010	50	
9			X			X			X	3	13,132	0.0321	0	
10	X				X	X			X	3	4,901	0.0051	1393	
11		X			X	X			X	3	472	0.0010	53	
12			X		X	X			X	3	12,010	0.0295	0	
13	X				X			X		3	4,472	0.0026	1575	Figures 12 & 13 ; Stress & Displacement
14		X			X			X		3	379	0.0010	48	
15			X		X			X		3	10,019	0.0355	0	
16	X				X	X		X		3	4,541	0.0024	1451	
17		X			X	X		X		3	474	0.0010	57	
18			X		X	X		X		3	10,826	0.0282	0	
19	X			X					X	4	3,420	0.0031	1536	
20		X		X					X	4	379	0.0010	60	
21			X	X					X	4	7,765	0.0274	0	
22	X			X					X	2.5	8,026	0.0090	1567	
23		X		X					X	2.5	348	0.0010	34	

Los Alamos National Laboratory
LANSCE Division
Group LANSCE-1

Table 2; Results from Analysis of ANL 350 MHz, 3-Gap, β_g=.36 Spoke Resonator

Case Number	Boundary Conditions / Loads			Radial Endwall Stiffeners				Annular Endwall Stiffener		Wall Thick	σ_{max} Von Mises	δ_{max}	Flange Reaction Force	Comments
	Vacuum Loading	Displaced End	Leak Check	ANL EB-24003-X	Wrap Around Tips	T-Section	None	Yes	No	(mm)	(psi)	(inches)	(lbs.)	
24			X	X					X	2.5	16,102	0.0488	0	
25	X				X				X	4	3,054	0.0030	1517	
26		X			X				X	4	386	0.0010	61	
27			X		X				X	4	7,891	0.0268	0	
28	X				X				X	2.5	6,101	0.0084	1512	
29		X			X				X	2.5	365	0.0010	35	
30			X		X				X	2.5	13,305	0.0456	0	
31	X						X		X	3	23,731	0.0325	-	Figures 14 & 15; Verification Problem - Compare to Next Line
32	X						X		X	3	24,414	0.0272	-	Axi-Symetric 2-D Model, Figure 16
33	X			X					X	3	4,325	0.0056	-	Pie slice, symetric model, Figures 17 & 18

GeoStar 2.5 (256K Version) : z - [Main]

FIGURE 1
ANL 350 MHZ 3-GAP SPOKE CAVITY

GEOMETRY PER ANL EB-24003-X

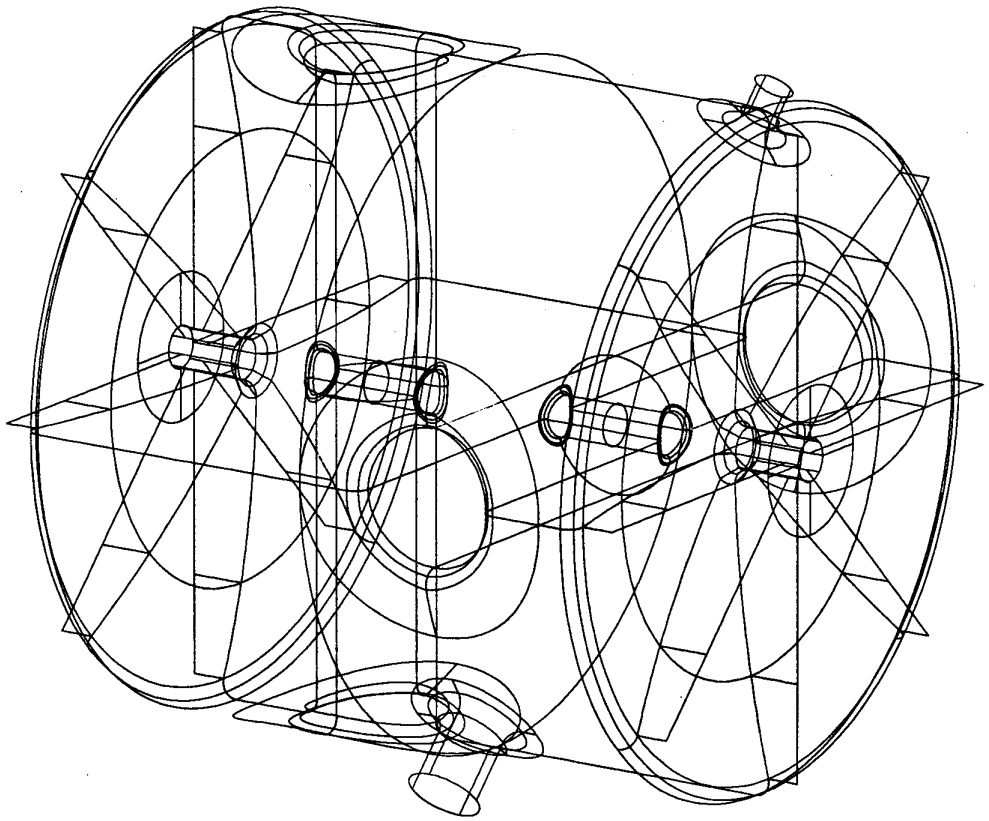

GeoStar 2.5 (256K Version) : z - [Main]

FIGURE 2

ANL 350 MHZ 3-GAP SPOKE CAVITY

WITH T SECTION WRAP-AROUND RADIAL END WALL STIFFENERS

WITH ANNULAR END WALL STIFFENER

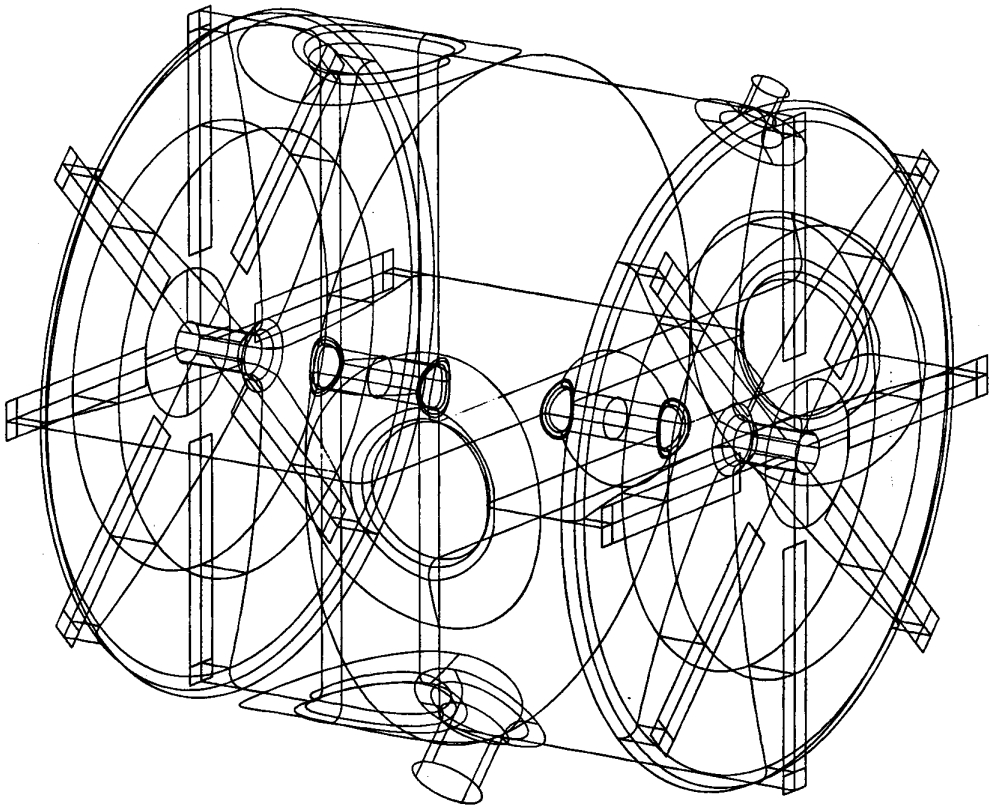

GeoStar 2.5 (256K Version) : z - [Main]

FIGURE 3

ANL 350 MHZ 3-GAP CAVITY ELEMENTS

GEOMETRY PER ANL EB-24003-X

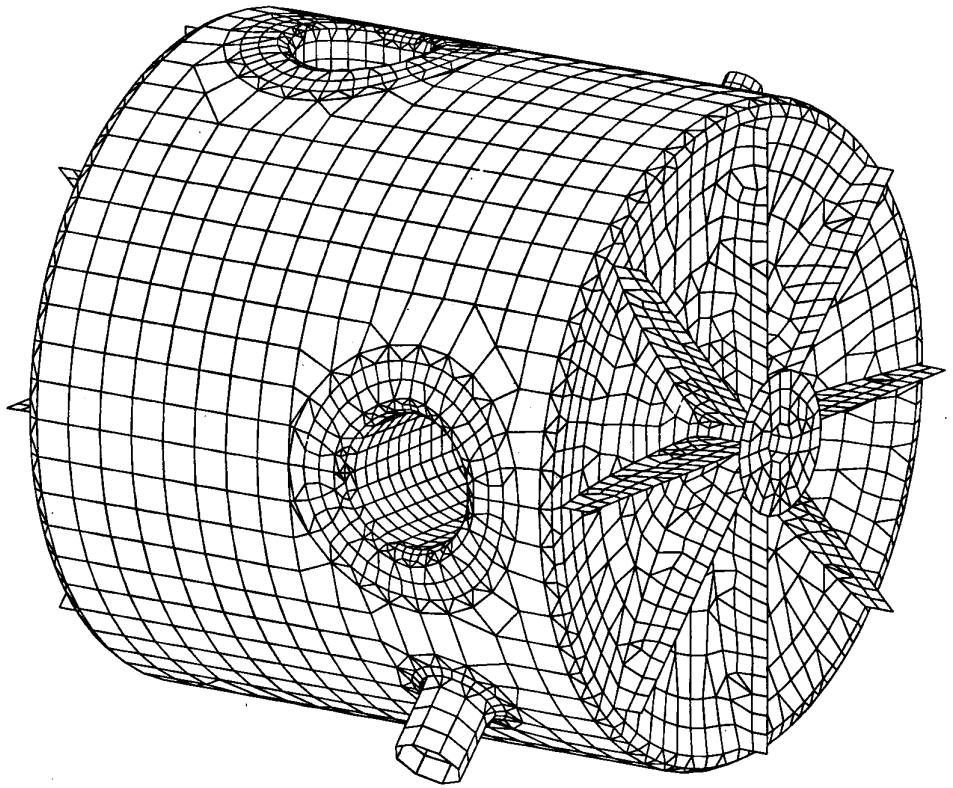

GeoStar 2.5 (256K Version) : z - [Main]

FIGURE 4

ANL 350 MHZ 3-GAP CAVITY ELEMENTS

WITH T SECTION WRAP-AROUND RADIAL END WALL STIFFENERS

WITH ANNULAR END WALL STIFFENER

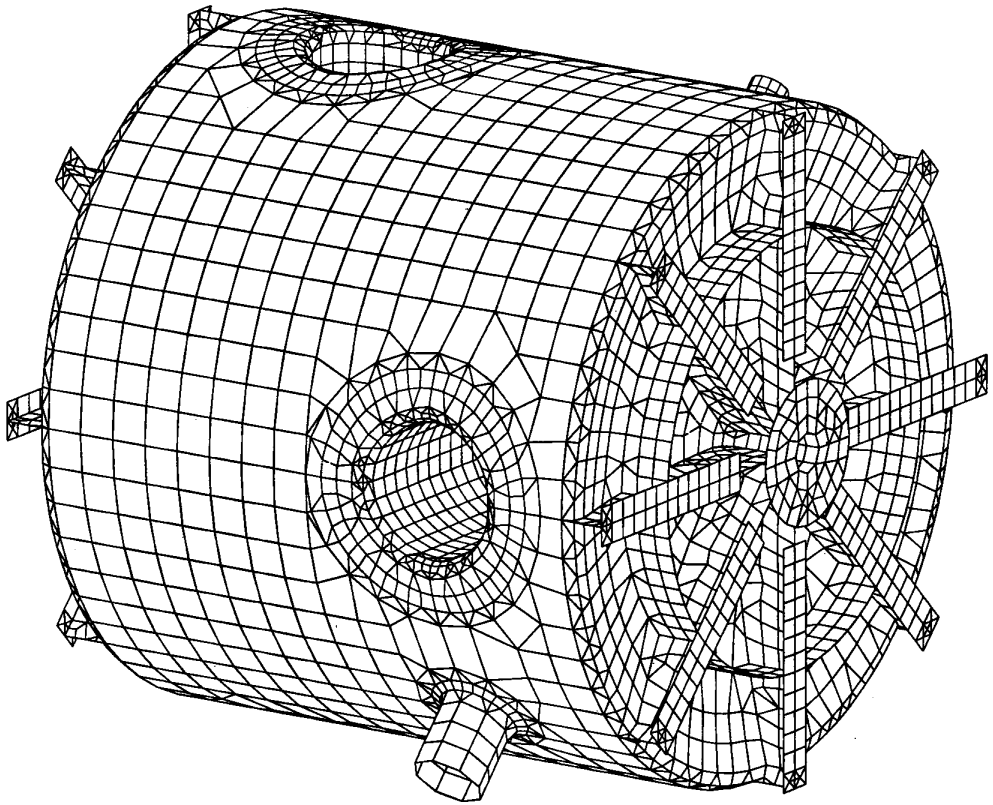

GeoStar 2.5 (256K Version) : z - [Main]

FIGURE 5

ANL 350 MHZ 3-GAP CAVITY ELEMENTS

NO STIFFENERS - VERIFICATION MODEL

FOR COMPARISON TO AXI-SYMETRIC MODEL

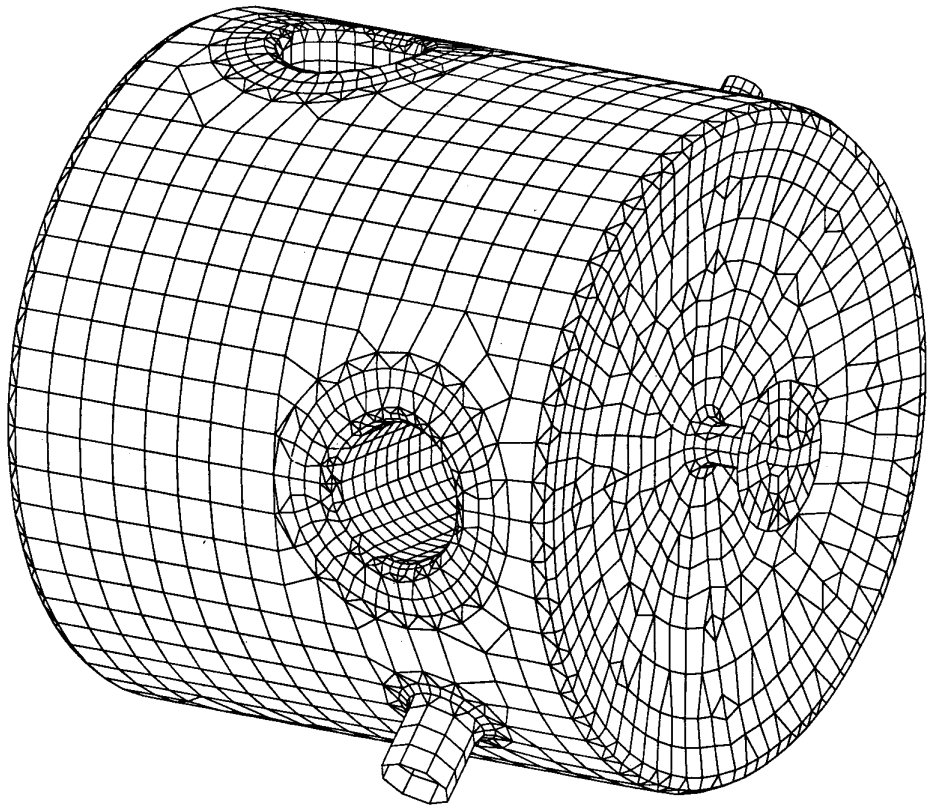

GeoStar 2.5 (256K Version): z - [Main]

Lin STRESS Lc=1

FIGURE 6

ANL 350 MHZ 3-GAP SPOKE CAVITY

VON MISES STRESS PLOT (PSI)

GEOMETRY PER ANL EB-24003-X

VACUUM LOADING

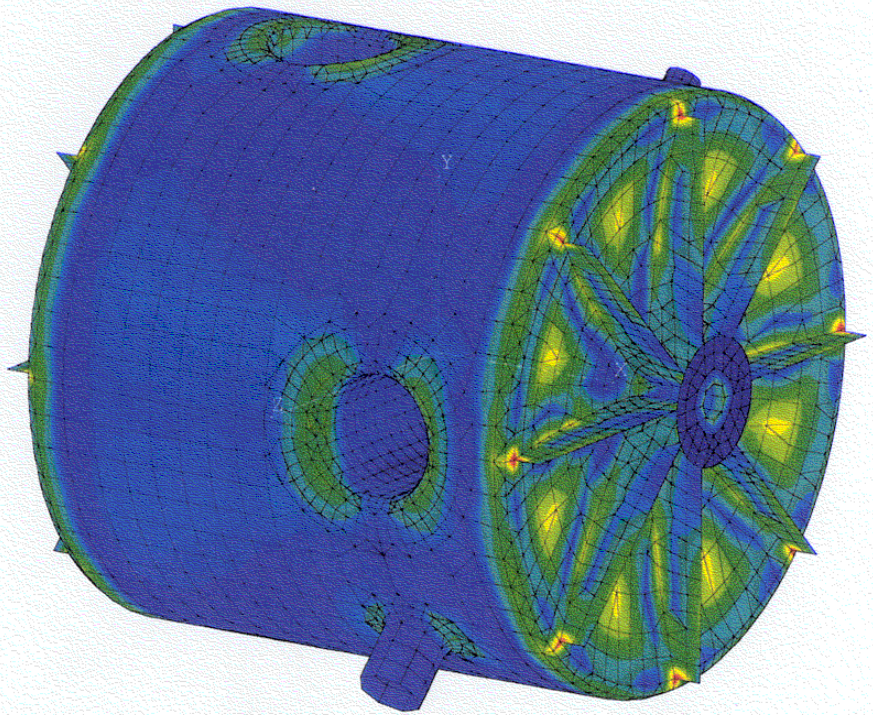

Von Mises

5822.800

5094.900

4367.100

3639.200

2911.400

2183.500

1455.700

727.8500

0.000000

GeoStar 2.5 (256K Version): z - [Main]

Lin DISP Lc=1

FIGURE 7
ANL 350 MHZ 3-GAP SPOKE CAVITY
RESULTANT DISPLACEMENT (INCHES)

GEOMETRY PER ANL EB-24003-X
VACUUM LOADING

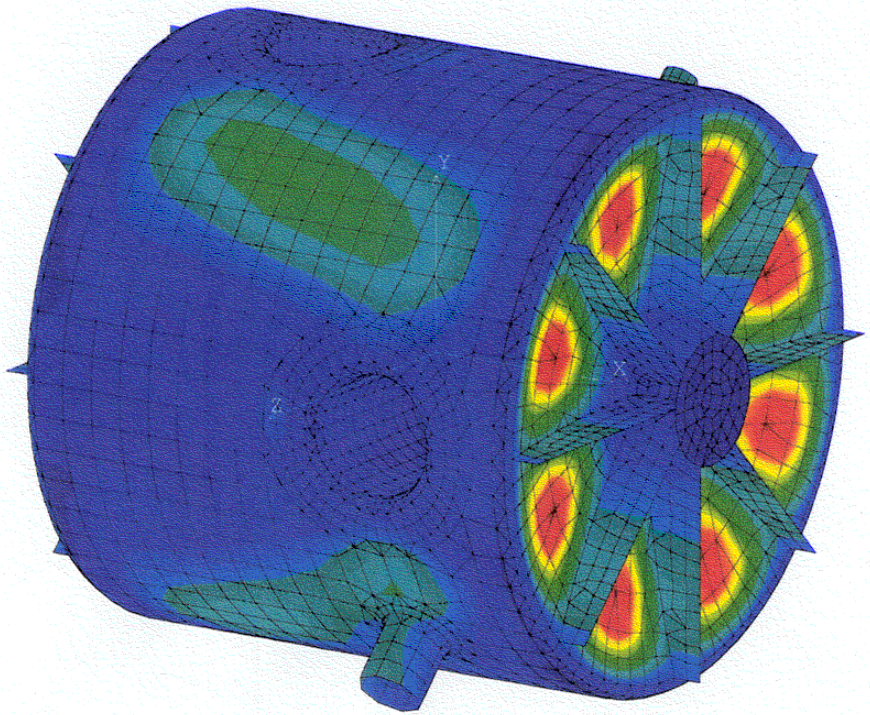

Disp_Res
0.00591980
0.00517990
0.00443990
0.00369990
0.00295990
0.00221990
0.00148000
0.00073998
1.000E-033

GeoStar 2.5 (256K Version): z - [Main]

Lin STRESS Lc=1

FIGURE 8
ANL 350 MHZ 3-GAP SPOKE CAVITY
VON MISES STRESS PLOT (PSI)

GEOMETRY PER ANL EB-24003-X + WRAP AROUND RADIAL ENDWALL STIFFENERS

VACUUM LOADING

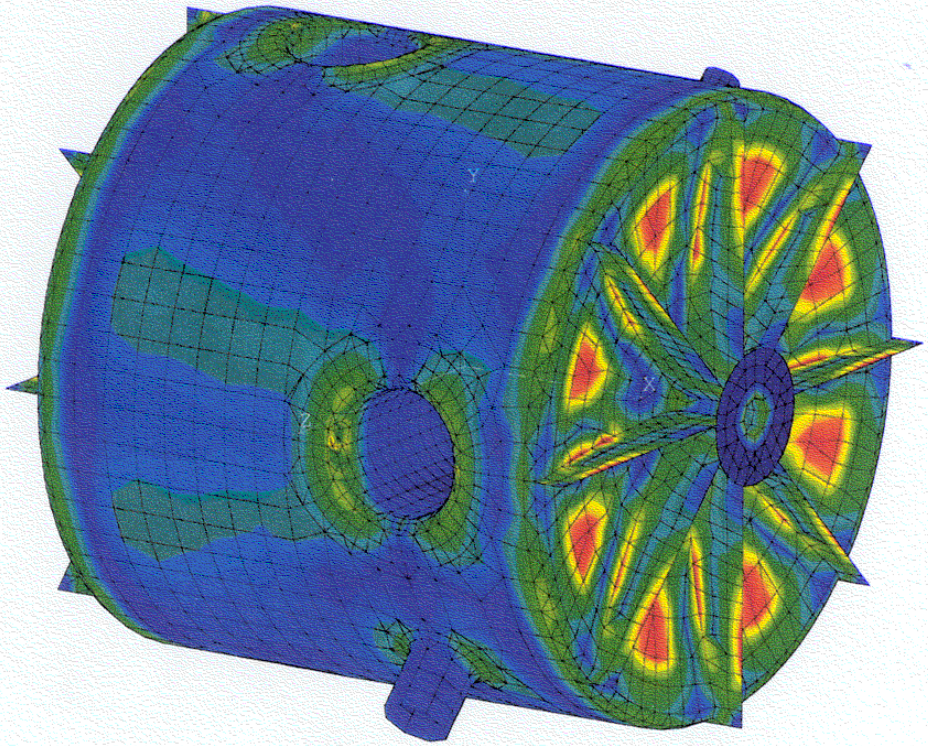

GeoStar 2.5 (256K Version): z - [Main]

Lin DISP Lc=1

FIGURE 9
ANL 350 MHZ 3-GAP SPOKE CAVITY
RESULTANT DISPLACEMENT (INCHES)

GEOMETRY PER ANL EB-24003-X + WRAP AROUND RADIAL ENDWALL STIFFENERS

VACUUM LOADING

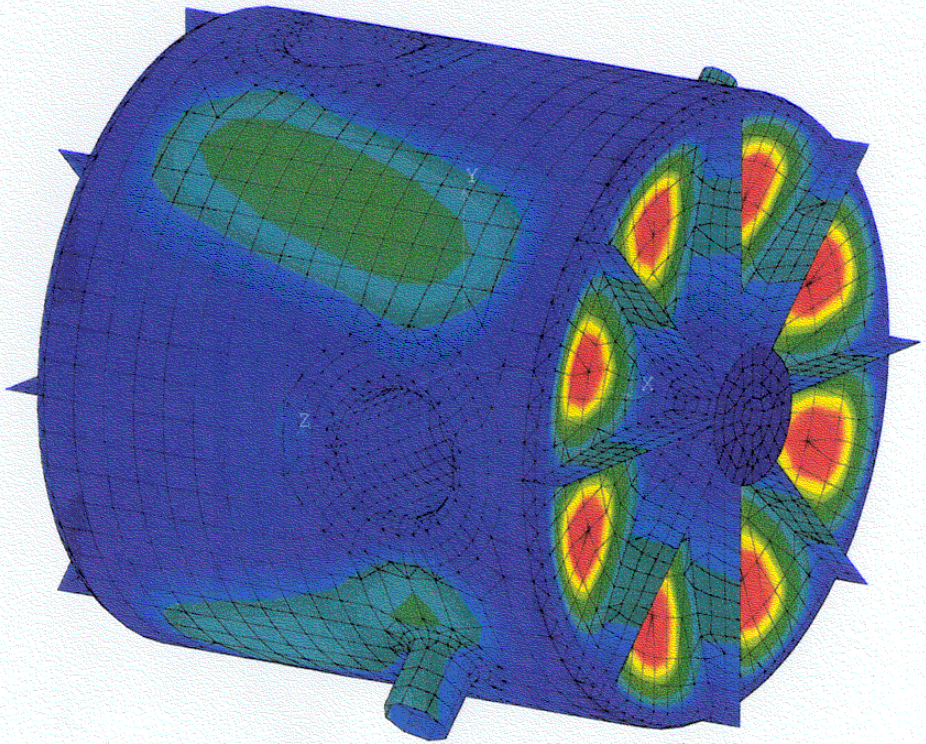

Disp_Res
0.00558060
0.00488300
0.00418550
0.00348790
0.00279030
0.00209270
0.00139520
0.00069758
1.000E-033

GeoStar 2.5 (256K Version): z - [Main]

Lin STRESS Lc=1

FIGURE 10
ANL 350 MHZ 3-GAP SPOKE CAVITY
VON MISES STRESS PLOT (PSI)

GEMETRY PER ANL EB-24003-X + T SECTION RADIAL ENDWALL STIFFENERS
VACUUM LOADING

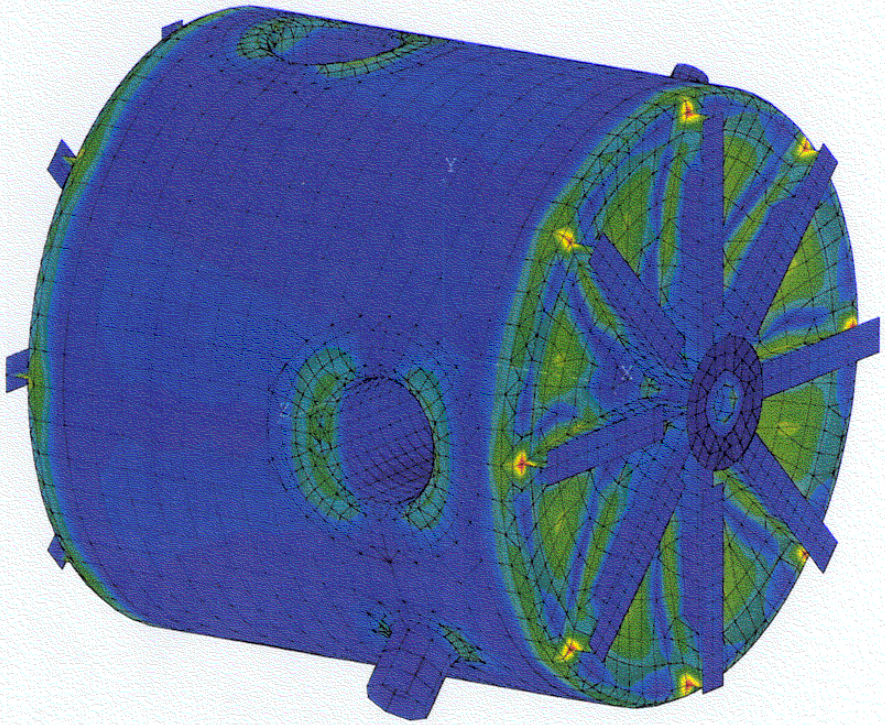

Von Mises
6845.100
5989.500
5133.800
4278.200
3422.500
2566.900
1711.300
855.6400
0.000000

GeoStar 2.5 (256K Version): z - [Main]

Lin DISP Lc=1

FIGURE //

ANL 350 MHZ 3-GAP SPOKE CAVITY

RESULTANT DISPLACEMENT (INCHES)

GEMETRY PER ANL EB-24003-X + T SECTION RADIAL ENDWALL STIFFENERS

VACUUM LOADING

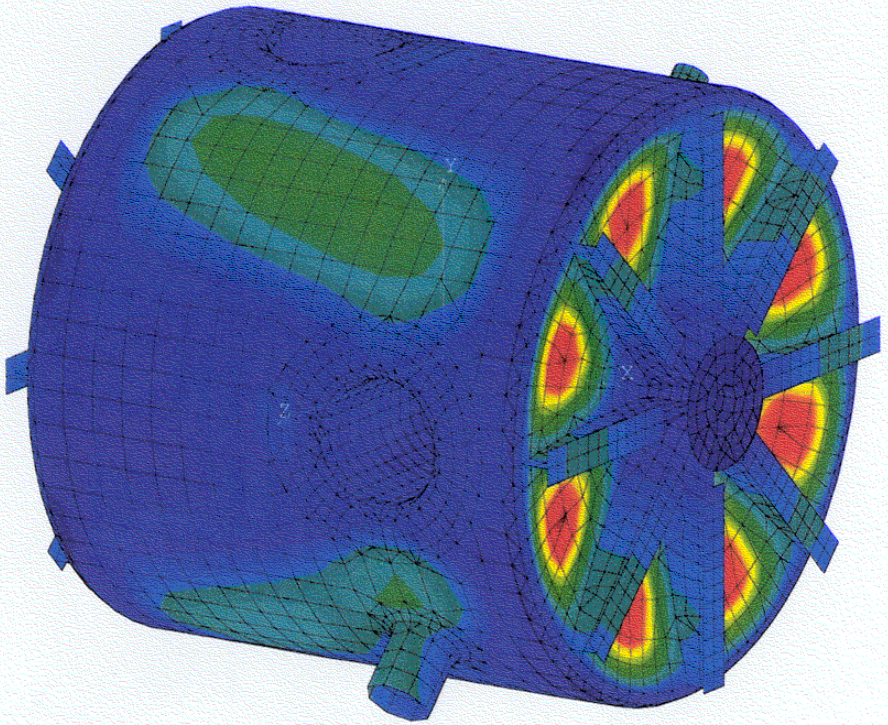

GeoStar 2.5 (256K Version) : z - [Main]

Lin STRESS Lc=1

FIGURE 12

ANL 350 MHZ 3-GAP SPOKE CAVITY

VON MISES STRESS PLOT (PSI)

GEOMETRY PER ALN EB-24003-X

+ WRAP AROUND RADIAL ENDWALL STIFFENERS

+ ANNULAR ENDWALL STIFFENER

VACUUM LOADING

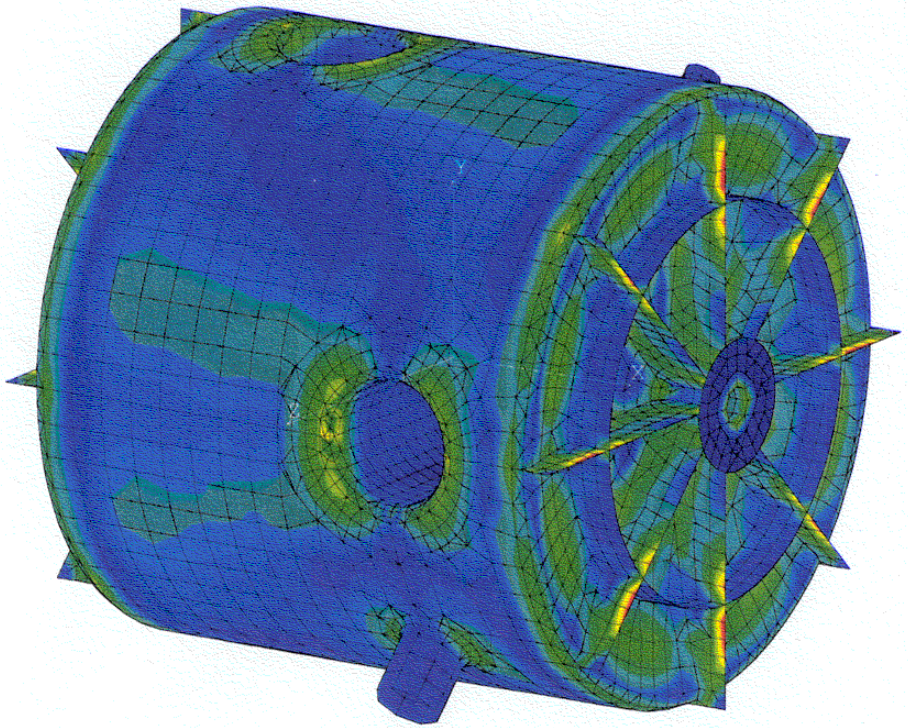

Von Mises

4472.800

3913.700

3354.600

2795.500

2236.400

1677.300

1118.200

559.1000

0.000000

GeoStar 2.5 (256K Version) : z - [Main]

Lin DISP Lc=1

FIGURE 13

ANL 350 MHZ 3-GAP SPOKE CAVITY

RESULTANT DISPLACEMENT (INCHES)

GEOMETRY PER ALN EB-24003-X

+ WRAP AROUND RADIAL ENDWALL STIFFENERS
+ ANNULAR ENDWALL STIFFENER

VACUUM LOADING

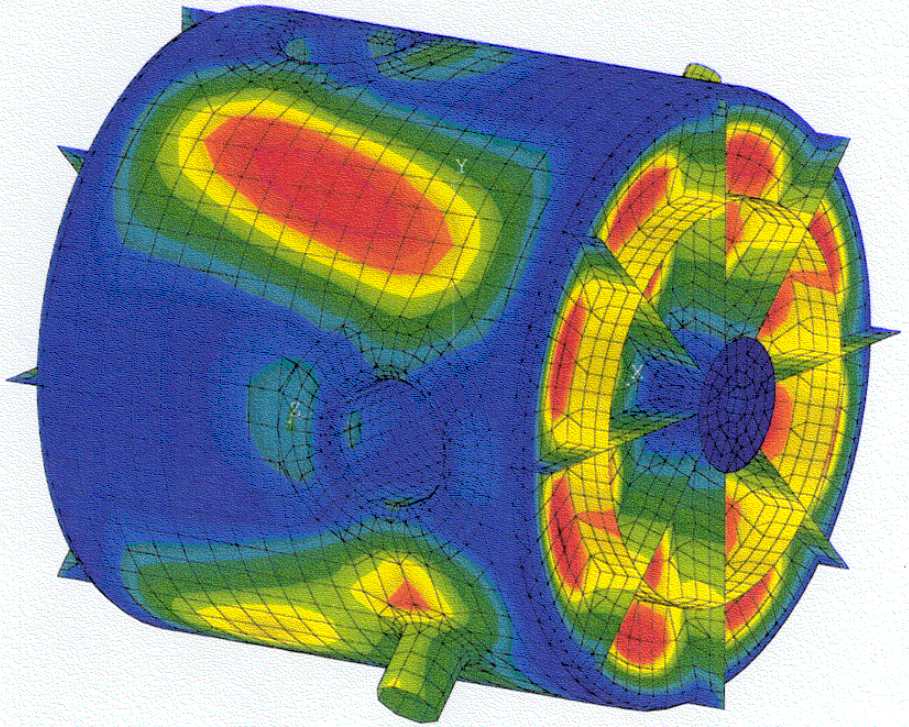

Disp_Res

0.00263090
0.00230210
0.00197320
0.00164430
0.00131550
0.00098661
0.00065774
0.00032887
1.000E-033

GeoStar 2.5 (256K Version): z - [Main]

Lin STRESS Lc=1

FIGURE 14

ANL 350 MHZ 3-GAP SPOKE CAVITY

VON MISES STRESS PLOT (PSI)

VERIFICATION PROBLEM

NO STIFFENERS

VACUUM LOADING

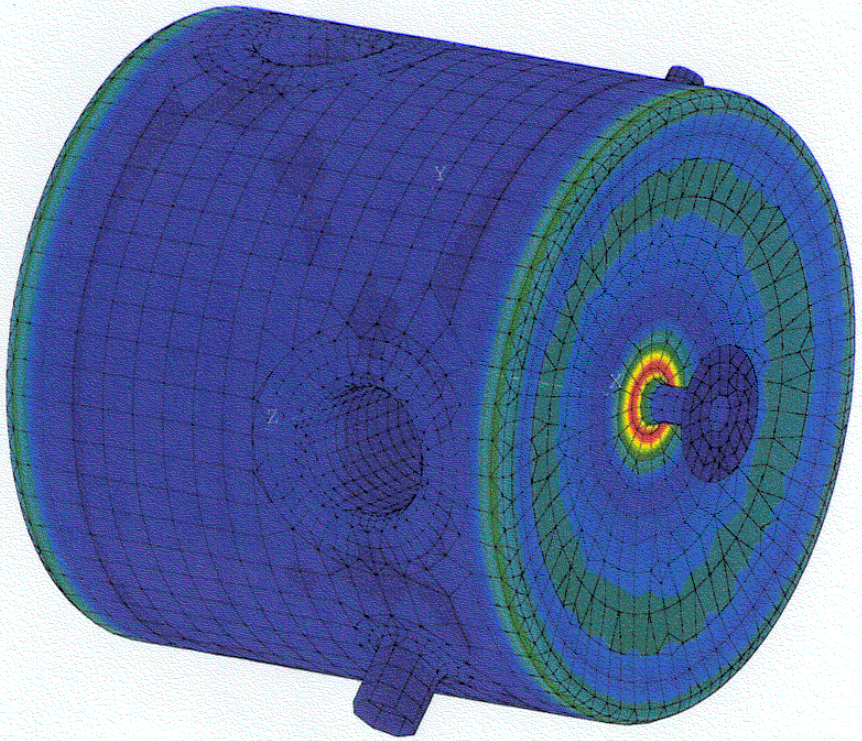

Von Mises

23731.00

20764.00

17798.00

14832.00

11865.00

8899.000

5932.600

2966.300

0.000000

GeoStar 2.5 (256K Version): z - [Main]

Lin DISP Lc=1

FIGURE 15

ANL 350 MHZ 3-GAP SPOKE CAVITY

RESULTANT DISPLACEMENT (INCHES)

VERIFICATION PROBLEM

NO STIFFENERS

VACUUM LOADING

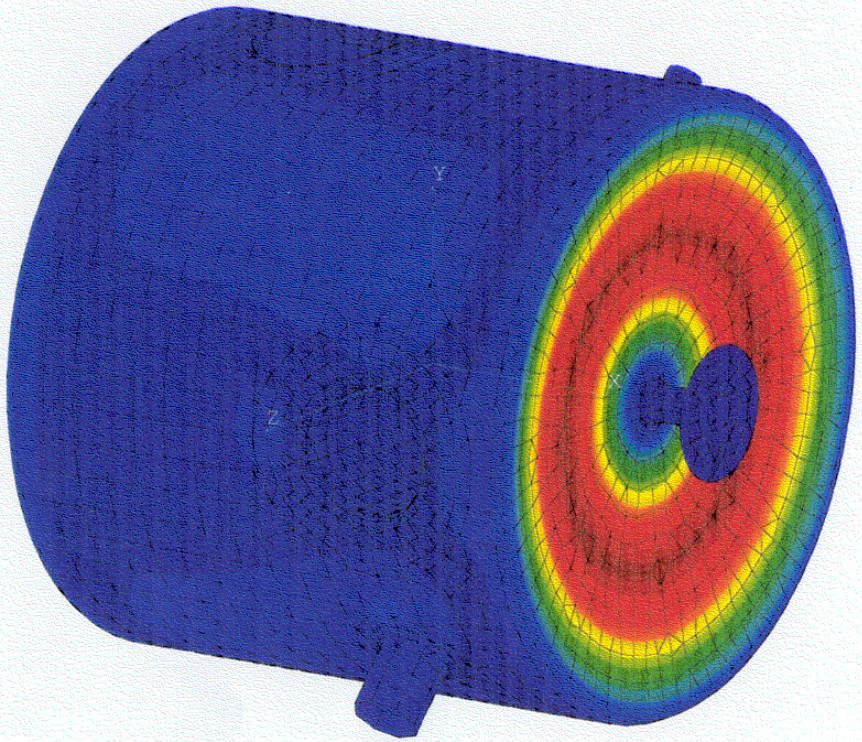

Disp_Res

0.0325560
0.0284870
0.0244170
0.0203480
0.0162780
0.0122090
0.0081391
0.0040696
1.00E-033

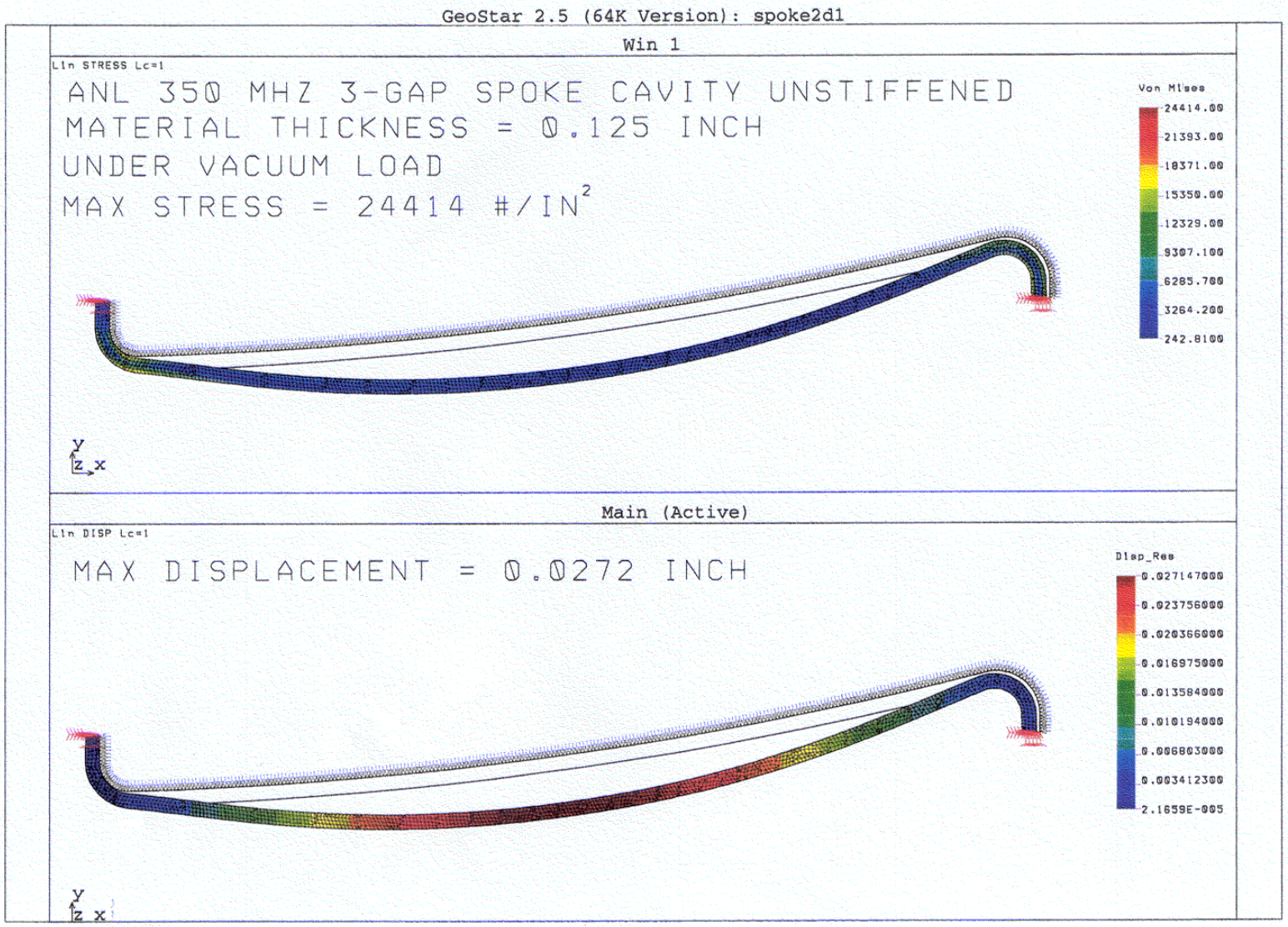
GeoStar 2.5 (64K Version): spoke2d1
Win 1
Lin STRESS Lc=1
ANL 350 MHZ 3-GAP SPOKE CAVITY UNSTIFFENED
MATERIAL THICKNESS = 0.125 INCH
UNDER VACUUM LOAD
MAX STRESS = 24414 #/IN2
Von Mises
24414.00
21393.00
18371.00
15350.00
12329.00
9307.100
6285.700
3264.200
242.8100
Y
Z X
Main (Active)
Lin DISP Lc=1
MAX DISPLACEMENT = 0.0272 INCH
Disp_Res
0.027147000
0.023756000
0.020366000
0.016975000
0.013584000
0.010194000
0.006803000
0.003412300
2.1659E-005
Y
Z X

FIGURE 16

GeoStar 2.5 (256K Version): z - [Main]

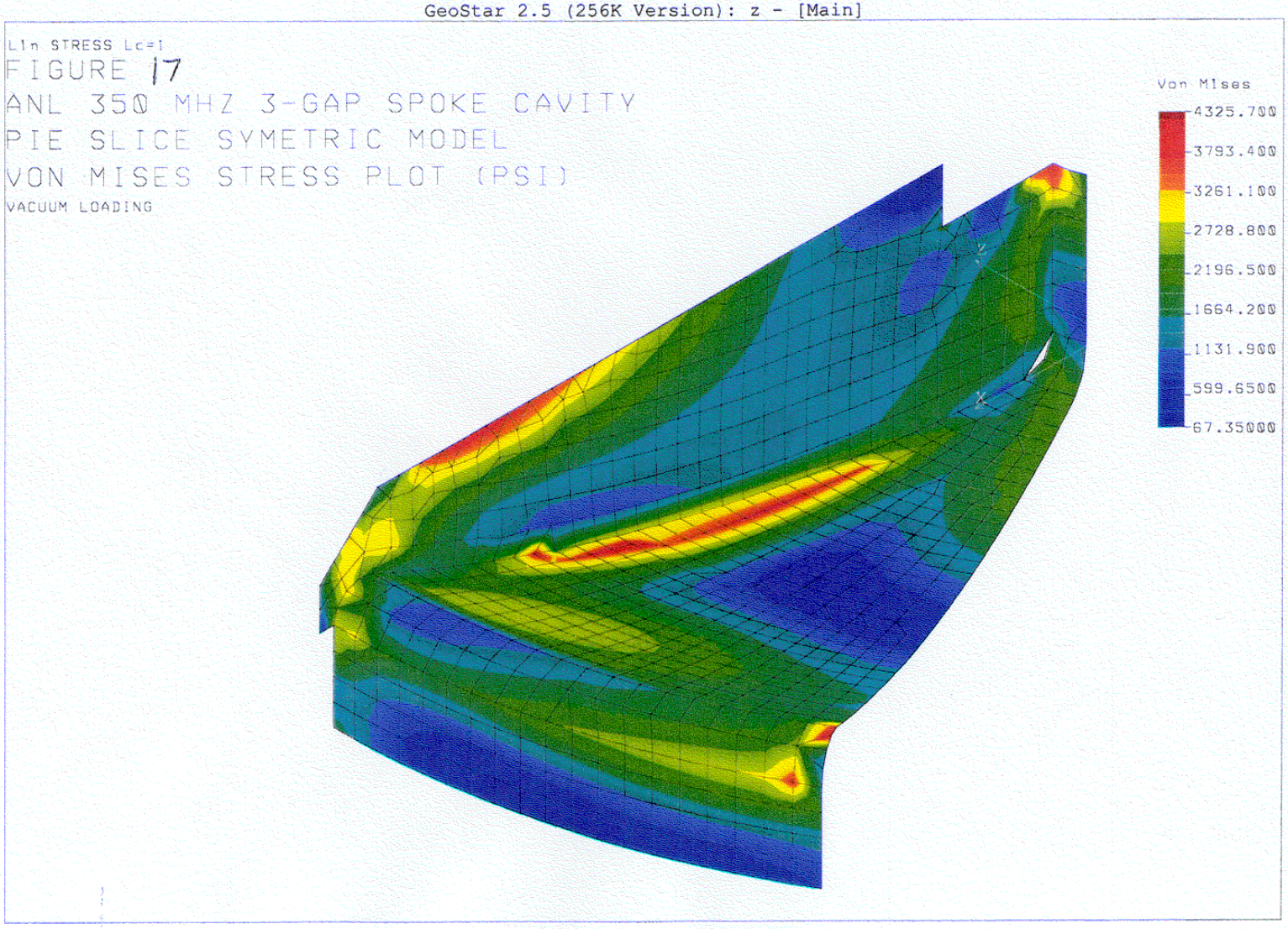

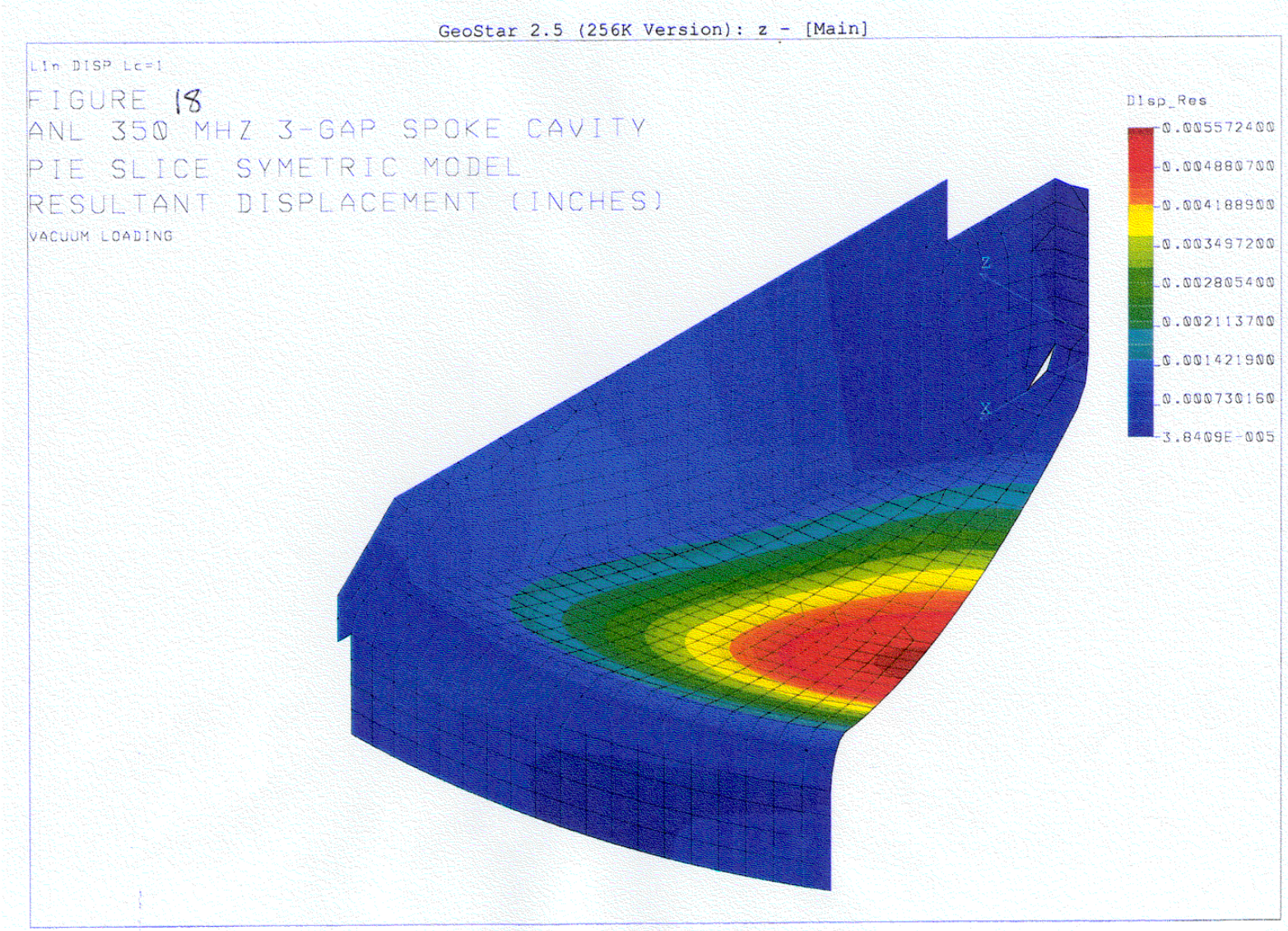
GeoStar 2.5 (256K Version): z - [Main]
Lin DISP Lc=1
FIGURE 18
ANL 350 MHZ 3-GAP SPOKE CAVITY
PIE SLICE SYMETRIC MODEL
RESULTANT DISPLACEMENT (INCHES)
VACUUM LOADING
Disp_Res
0.005572400
0.004880700
0.004188900
0.003497200
0.002805400
0.002113700
0.001421900
0.000730160
3.8409E-005
Z
X

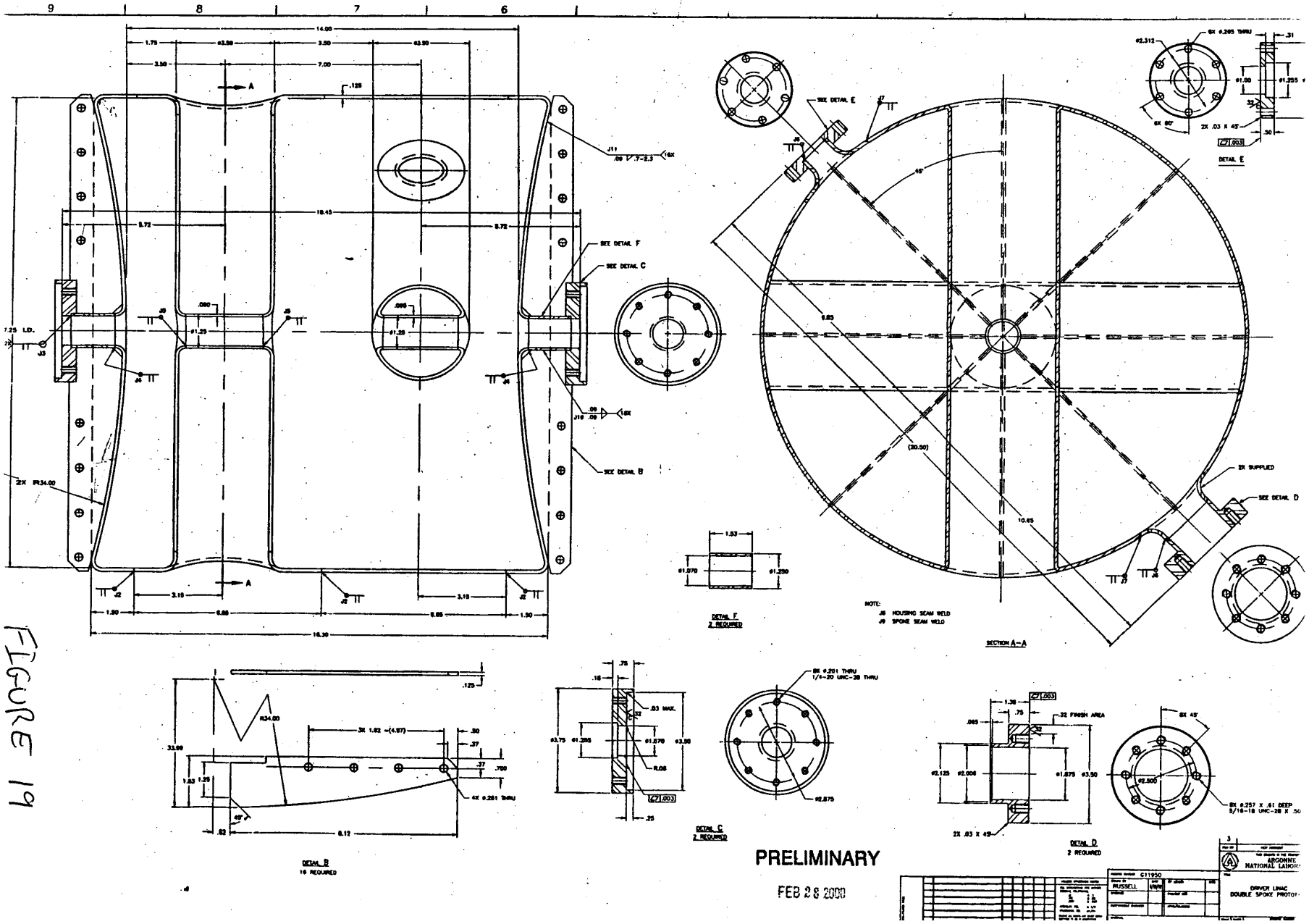
PRELIMINARY
FEB 28 2000
DETAIL B
10 REQUIRED
DETAIL C
2 REQUIRED
DETAIL D
2 REQUIRED
DETAIL E
DETAIL F
2 REQUIRED
SECTION A-A
NOTE:
J8 HOUSING SEAM WELD
J9 SPOKE SEAM WELD
SEE DETAIL B
SEE DETAIL C
SEE DETAIL D
SEE DETAIL E
SEE DETAIL F
8X SUPPLIED
ARGONNE NATIONAL LABOR
DRIVER LINAC
DOUBLE SPOKE PROTOT

FIGURE 19

CC:
B. Baillie, LANSCE-1, MS H817
K. Bongardt, Forschungszentrum Jülich
D. Bruhn, LANSCE-1, MS H817
M. Cappiello, APT-TPO, MS H816
K. C. Chan, APT/TPO, MS H816
R. Garnett, LANSCE-1, MS H817
R. Gentzlinger, ESA-DE, MS H821
D. Gilpatrick, LANSCE-1, MS H817
H. Haagenstad, LANSCE-1, MS H817
W. B. Haynes, LANSCE-9, MS H851
A. Jason, LANSCE-1, MS H817
M. Johnson, Cornell Univ.
M. Kedzie, ANL
P. Kelley, LANSCE-1, MS H817
F. Krawczyk, LANSCE-1, MS H817
G. Lawrence, APT/TPO, MS H816
J. Ledford, LANSCE-1, MS H817
P. Leslie, LANSCE-1, MS H817
P. Lisowski, APT-PDO, MS H813
R. Lujan, LANSCE-1, MS H817
F. Martinez, LANSCE-1, MS H817
K. Meunier, Sunwest Cad
J. Mitchell, LANSCE-1, MS H817
D. Montoya, LANSCE-1, MS H817
A. Naranjo, LANSCE-1, MS H817
J. O'Hara, Honeywell, MS H817
P. Ostronouv, ANL
N. Patterson, LANSCE-1, MS H817
H. Padamsee, Cornell Univ.
A. Rendon, LANSCE-1, MS H817
P. Roybal, LANSCE-1, MS H817
R. Roybal, LANSCE-1, MS H817
L. Rybarcyk, LANSCE-1, MS H817
E. Schmierer, ESA-DE, MS H821
S. Schriber, LANSCE-DO, MS H845
A. Shapiro, LANSCE-1, MS H817
R. Sheffield, APT-TPO, MS H816
K. Shepard, ANL
F. Sigler, LANSCE-1, MS H817
J. Szalczinger, LANSCE-1, MS H817
T. Tajima, LANSCE-1, MS H817
R. Valdiviez, LANSCE-1, MSH817
T. Wangler, LANSCE-1, MS H817
R. Wood, LANSCE-1, MS H817
T. Wright, LANSCE-1, MS H817
L. Young, SNS, MS H817
LANSCE-1 Reading File, MS H817